Research Article

Selective Signal Suppression in Traveling Wave MPI: Focusing on Areas with Low Concentration of Magnetic Particles

Stefan Herz[a,*] · Patrick Vogel[a,b] · Thomas Kampf[b,c] · Martin A. Rückert[b] · Volker C. Behr[b] · Thorsten A. Bley[a]

[a]Department of Diagnostic and Interventional Radiology, University Hospital Würzburg, Würzburg, Germany
[b]Department of Experimental Physics 5 (Biophysics), University of Würzburg, Würzburg, Germany
[c]Department of Diagnostic and Interventional Neuroradiology, University Hospital Würzburg, Würzburg, Germany
*Corresponding author, email: herz_s@ukw.de

Abstract

Many MPI scanners have difficulties to correctly visualize areas with a broad signal intensity spectrum due to their low signal dynamic capability. This effect is caused by analog-digital-converters (ADC) which are required for digitizing raw analog signals and are limited in their dynamic range. In Lissajou-trajectory MPI scanners this issue can be addressed by scanning small patches out of a large field of view (FOV) and adjusting the dynamic range for every patch separately. In traveling wave MPI (TWMPI) an elongated dynamic linear gradient array (dLGA) is used for the generation of field free points allowing to scan a relatively large FOV with a relatively short acquisition time. To date the patch concept cannot easily be transformed to TWMPI. However, the signal can be selectively suppressed by locally reducing the speed of the FFPs due to the modular design of the TWMPI scanner. In this study a dynamic drive field forming technique for TWMPI is introduced which allows to focus on low SPIO concentrations in samples with a large range of tracer concentrations. This could facilitate preclinical functional imaging in the proximity of organs with high unspecific SPIO uptake such as the liver.

I. Introduction

Functional imaging with MPI using targeted or non-targeted superparamagnetic nanoparticles (SPIOs) is a promising tool for preclinical biomedical imaging. So far, many MPI scanners have difficulties to correctly visualize areas with a broad signal intensity spectrum due to their low signal dynamic capability [1, 2]. MPI linearity experiments were commonly performed with only one sample in the field of view (FOV). Hence, a wide range of signal values of up to $\sim 10^5$ was resolved. Studies that investigated multiple samples in the FOV, however, reported a much smaller range of particle concentrations [1]. As a consequence, the high unspecific uptake of nanoparticles by reticuloendothelial organs such as liver or spleen can mask lower concentrations of specific SPIO clusters in the proximity.

The signal generated in an MPI scanner grows linearly with the concentration of the imaged particle system. Low particle concentrations can be detected since the receive chain of an MPI system is optimized for high sensitivity featuring low physical noise levels. The raw analog signal is digitized using an analog-digital-converter (ADC). An ADC comes with the limitation of dynamic range, which is the capability resolving the amplitude of an incoming analog signal. The effective number of bits (ENOB) for common ADCs is in the range of 8 to 32 bit depending on their effective converting speed or

sampling rate (SR)[1]. The noise level in an optimal receive chain should lie over the least significant bit (LSB), which allows increasing the signal-to-noise (SNR) ratio of the acquired signal by averaging. However, simultaneous imaging of high and low particle concentrations requires a change of the dynamic range settings [3] fitting the entire signal, which can be done by adjusting the low noise pre-amplifier (LNA) in the receive chain. This causes the effect that signal with an amplitude in the range of the noise level such as in a low concentrated point sample falls below the LSB line, where it cannot be digitized anymore (Fig. 1 b). Thus, simultaneous imaging of two point samples with different concentrations is limited to a certain concentration spread (Fig. 1 b and c).
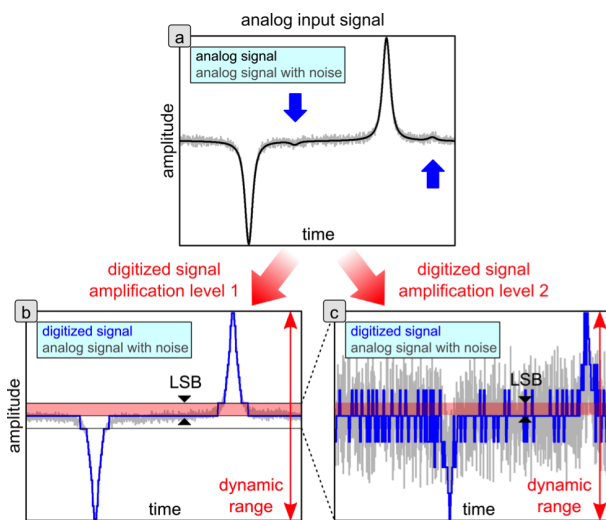
Figure 1: (a) Simulation of a raw analog MPI signal (with and without noise) containing two point samples with high and low signal intensity, respectively (the sample with low signal is indicated by blue arrows). (b) While the continuous analog signal contains all information, the digitized signal using an ADC only yields discrete steps leading to the disappearance of the signal variations lower than the LSB size. (c) By suppressing the higher signal, the amplification level can be adjusted fitting the dynamic range of the ADC distinguishing the low signal from noise.

For MPI scanners working with Lissajous trajectories [4] this issue can be addressed scanning small patches out of a large field of view (FOV) [5], which allows adjusting the dynamic range for every patch separately. Scanning slices out of a 3D volume, which is the case in field-free line systems, also allows a suitable adjustment of the dynamics [6]. Nevertheless, within a scanned area it is not possible to accurately visualize low signal in the presence of high signal.

A traveling wave MPI system (TWMPI) provides a huge FOV, which is scanned at once [7–9]. Due to the modular hardware design of the traveling wave MPI sys-

tem, it is possible to arbitrarily modify the trajectory of the field free points (FFPs) in an easy way.

In this simulation study a selective signal suppression technique is presented using an advanced trajectory design to reduce the issue of dynamic range for TWMPI systems.

II. Methods

Simulations were performed for a traveling wave MPI (TWMPI) scanner providing a FOV of $65 \times 29 \times 29$ mm^3 and working at frequencies of $f_1 = 920$ Hz and $f_2 = 16823$ kHz [6]. A custom-made simulation environment emulating a real TWMPI scanner (with noise and 8 bit ADC simulation) [10] was used. For all simulations the noise level was identical. The range of the ADC was adapted to the maximum simulated signal range. For reconstruction a system matrix based approach was applied [11].
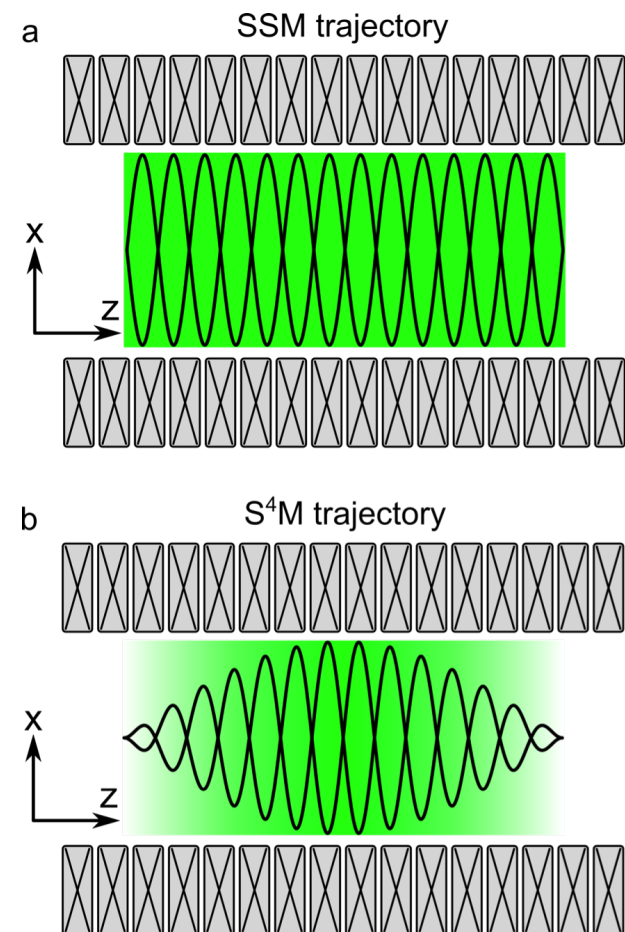
Figure 2: Sketch of the trajectory of FFPs in TWMPI (a) Slice-scanning mode (b) Signal suppressing slice-scanning mode (S^{4}M) using a sinusoidal modulated amplitude. The green shades indicate the amount of signal received.

TWMPI differs from other MPI scanners in signal generation and encoding by using an elongated dynamic

linear gradient array (dLGA) for the generation of field free points [7–9]. Generally, for suppressing signal intensity the speed of the moving FFPs has to be decreased [12]. Due to its modular design the TWMPI scanner setup allows to modify the trajectory of the FFPs easily. In the so called slice-scanning mode (SSM) the FFPs travel on a planar sinusoidal trajectory through the field of view (Fig. 2 a). The shape of the trajectory is given by the frequency f_1 of the dLGA for motion in z-direction and the frequency f_2 ($f_2 \gg f_1$) of a saddle coil system for motion in x-direction perpendicular to the dLGA [7–9]. The deflection of the FFPs' trajectory in x-direction and hence the speed of the FFPs is controlled via the saddle coils. Reducing the current in the saddle coils results in a decreased speed of the FFPs and thus a reduced signal. Furthermore, the trajectory can be modified not to cover certain areas inside the FOV anymore. In Fig. 2 b a simple trajectory modification is indicated, where the amplitude is modulated with the sinus frequency $f_3 = f_1$. This modification allows reducing signal acquired from areas excited with smaller amplitudes. The resulting sequence is called signal suppressing slice-scanning mode (SSSSM = S^{4}M).

II.I. General shape-function

A simple sinusoidal modulation of the amplitude as indicated in Fig. 2 b can only suppress signal generation in the outer range of the FOV. In addition, the position as well as the strength of the suppression can be set with a general shape-function (sf) following the formula:

$$sf(n, k, \varphi) = \left| \sin^n(\pi k f_1 + \varphi) \right|, \qquad (1)$$

where the exponent n gives the dimension of the suppression, k represents the number of waves, and φ is used to move the pattern along the z-direction. This allows suppression of slices perpendicular to the z-direction.

II.II. Phase dependency

In Fig. 3 the influence of the phase φ on the trajectory with $n = 3$ and $k = 1$ is indicated. By changing the phase the position of the area with the highest signal attenuation can be selected, which allows for separating areas of higher and lower signal acquisition in the FOV of the scanner.

II.III. Wavenumber dependency

By increasing the wavenumber k the number of areas for high signal acquisition can be increased within the FOV. In Fig. 4 the trajectories for $n = 3$ and $k = 2$ and $k = 3$ respectively are shown. It is also possible to combine the phase and the wavenumber dependency to select the sensitive area more precisely.
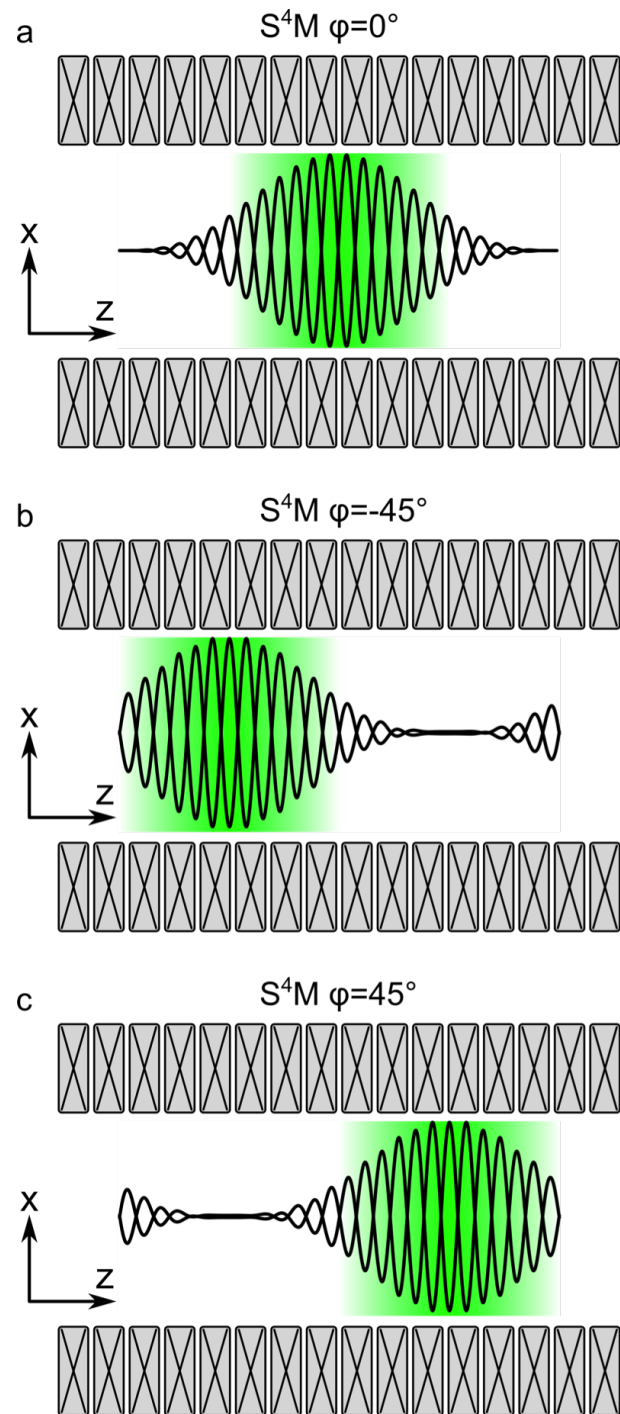
Figure 3: Sketches show the influence of phase φ on the trajectory inside the scanner with the shape-function $sf(3, 1, \varphi)$. By changing phase φ the position can be modified. The green shades indicate the amount of signal received.

III. Results

To demonstrate the functional principle of selective signal suppression two point samples with different concentration ratios were simulated. Both samples were assem-
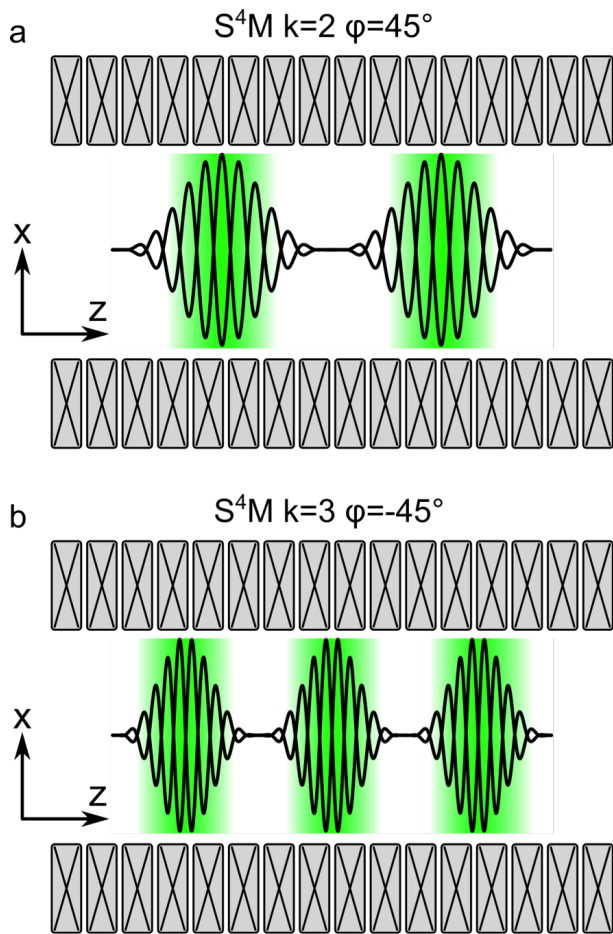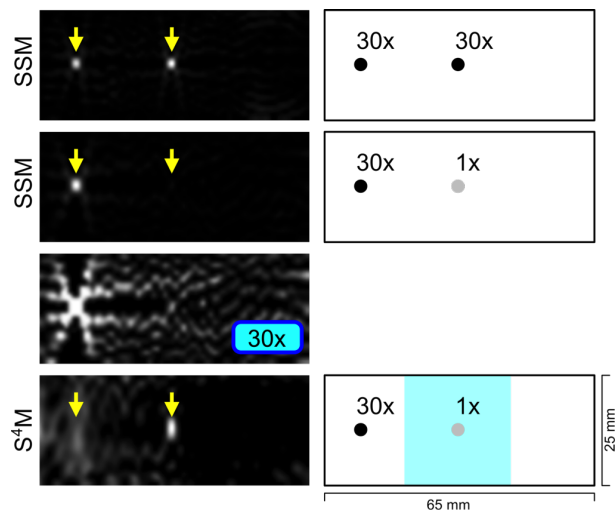
Figure 4: Sketches of the trajectories with different wavenumbers k ($n = 3$). With higher wave numbers k the quantity of high signal acquisition areas increases.

Figure 5: Reconstructed images of two point samples ($n = 3$, $k = 1$, $\varphi = 0°$) in simulated data. First and second row: SSM with different concentrations. Third row: 30 fold increased signal intensity (SSM) to investigate scaling effects. The sample on the right is blurred by noise. Bottom row: S⁴M approach decreases the strong signal from the sample with the high concentration on the left and unmasks the lower concentrated sample on the right. Signal intensity was separately adjusted for each image.
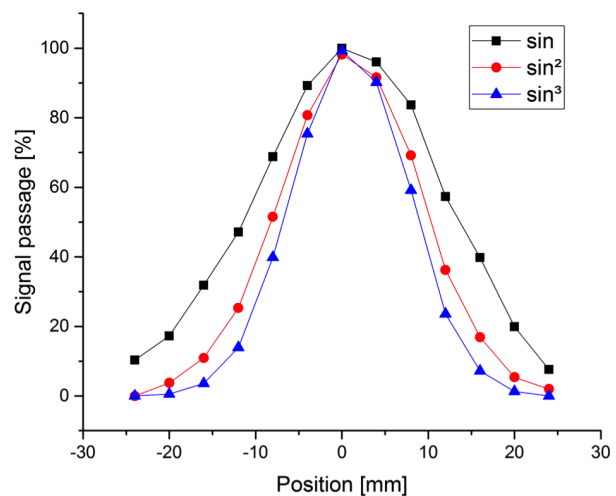
bled in a distance of 15 mm. In Fig. 5 the first row shows two samples with an equal concentration using SSM. In the second row the concentration of the right sample is reduced by 97 %. In the corresponding SSM-scan the signal of the lower concentrated sample cannot be reliably detected because of limits in dynamic range. The third row features both samples with a 30 fold increased signal intensity to investigate scaling effects. Here, the signal of the low concentrated sample cannot be distinguished from noise with certainty. Using the S⁴M approach ($n = 3$, $k = 1$, $\varphi = 0°$, bottom row) the signal from the higher concentrated point sample is suppressed whereas the lower concentrated sample is clearly revealed.

The graph in Fig. 6 demonstrates the signal suppression for shape-functions with different numbers n ($n = 1, 2, 3$) in contrast to the unshaped SSM sequence[2]. As expected, the signal decreases around the center of the sensitive area with the corresponding sinusoidal shape. Applying a sin³-shape leads to a suppression of the signal to about 90 % in a distance of 15 mm from the center.

_____
[2]For signal determination raw images were used.

Figure 6: Signal intensity for shape-functions with $n = 1$, $n = 2$, and $n = 3$ around the center of the sensitive area.

Different phases lead to a change in position of the sensitive area. For further investigation this effect was simulated in a phantom with three different signal letters using $n = 3$, $k = 1$, and $\varphi = -45°/0°/+45°$. In Fig. 7 these images are presented. S⁴M with different φ suppresses the corresponding letters. However, the signal from neighboring letters is still traceable in the transition areas of the reconstructed images and can appear as vertical line artifact.

In Fig. 8 the effect of wave number dependency is investigated in a simulation with 5 sample points using a
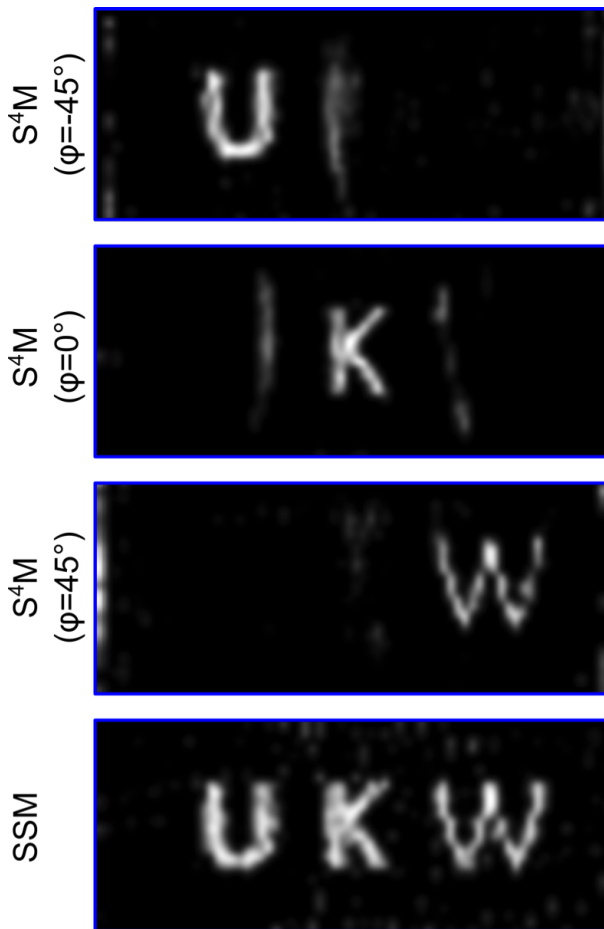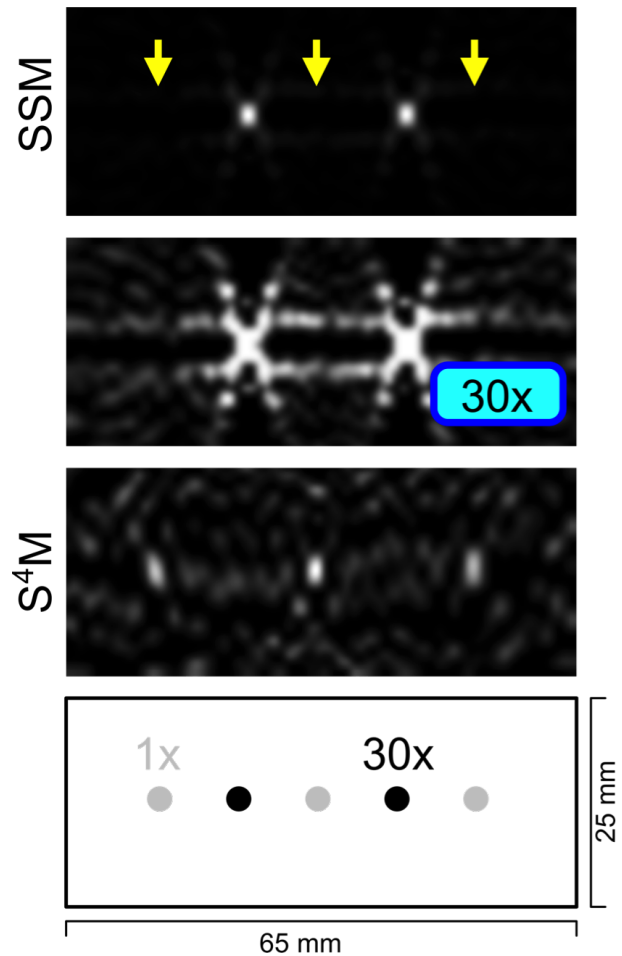
Figure 7: Simulation of selective signal suppression by changing phases in the S4M sequence in each row. Different phases lead to the suppression of corresponding areas in the FOV. In all case the FFP moves through the entire FOV along the z-axis but acquires only selected region of interest.

Figure 8: Simulation of 5 point samples with a concentration ratio of $1:30:1:30:1$. By using the SSM sequence only the higher concentrated samples can be detected in the reconstructed image. Increasing the signal intensity 30 fold (second row) does not reveal the hidden point samples. In contrast, S^4M ($n = 3$, $k = 3$, and $\varphi = -45°$) reveals the lower concentrated samples.

concentration ratio of $1:30:1:30:1$. It is shown that by using the SSM only the two higher concentrated samples are visible in the reconstructed image. A modified S^4M sequence with the parameters $n = 3$, $k = 3$, and $\varphi = -45°$ was applied to suppress the two higher concentrated samples.

IV. Discussion

The main issue of resolving signal of particle samples with a wide range of concentrations is the limited dynamic range of the ADC. In theory, an n bit ADC provides a resolution of 2^n values for digitizing the entire amplitude (peak-to-peak). Thus, concentrations with a ratio of 1 to $(2^n/2) - 1$ are separable (Fig. 1). However, in reality the ENOB normally lies about 1 to 2 bits below the given bit value of the ADC. Additional effects like reconstruction issues, discretization effects of the point spread function (PSF) as well as the fact, that the ADC is not used in the entire dynamic range, also could reduce the capability of resolving high spreads of concentrations. The described effect does probably not only depend on the ADC but also on the distance of the point samples to each other [2].

The results in Fig. 5 demonstrate the reconstructed images of two particle samples for a concentration range of 1 to 30, which lies at the limits using a real 8 bit ADC providing a theoretical ratio of 1 to $(2^{(8-2)}/2) - 1 = 31$. In contrast to the S^4M approach standard SSM was not able to adequately visualize the low concentrated samples.

The data used for the signal suppression graph shown in Fig. 6 were extracted from raw images (before reconstruction). Using min/max values of the reconstructed images yielded an apparent signal suppression of about 25 % in the center. This is presumably accounted for by the deconvolution and reconstruction process [8, 9]. Due

to the utilization of the same simulated PSF for the reconstruction, in the case of a shaped sequence the PSF is changed in a way that it is compressed along the z-direction. This results in an apparently smaller signal amplitude.

The presented sequence only allows suppression of signal in planes perpendicular to the z-axis. This allows for separating signals with high dynamic range along the z-direction. If higher and lower signals are distributed in the x-direction in these planes, this modification cannot be applied to suppress the higher signal without simultaneously suppressing the lower one. To address this issue a more sophisticated modification is necessary, which has to use additional offset fields to deflect the traveling FFPs from the higher concentrated areas.

The extent of position-dependent signal suppression can be adjusted by the shape of the applied sinusoidal amplitude. So far only qualitative imaging with S^4M is possible. To investigate quantitative evaluation in S^4M further research focusing on the stability of signal suppression for all phase angles, n's and k's is necessary.

Another approach will be to acquire multiple scans with SSM and series of different S^4M scans from different areas of the FOV. Out of these data a high-definition (HD) image could be reconstructed, which could overcome the issue of low signal dynamic capability of MPI systems.

Technical implementation of the presented sequence faces challenges. A modulation as suggested has to be generated by the addition of two sin waves with a frequency difference of $k \cdot f_1$. By modulating the excitation chain the amplitude could drop distinctly depending on the modulation frequency. In this case (main frequency 1 kHz and modulation frequency 500 Hz) the amplitude could decrease by 90 %, which would make this sequence useless. To overcome this issue different approaches e.g. increasing the amplifier or the implementation of a double resonant excitation chain as it is known from MRI have to be investigated [13].

Shaping the trajectory in TWMPI can be useful to visually separate areas of high concentrated particles from low concentrated areas. However, signal in the transition area could be still visible (see Fig. 7) and come out with a distorted projection, e.g. a point sample is reconstructed as a line. Applying modified system matrices and a selective patch reconstruction [11] can be used to address this issue.

V. Conclusion

A selective signal suppression technique for TWMPI is introduced which allows to select areas with low SPIO concentration for focused visualization in samples with a large range of tracer concentration. This can facilitate preclinical functional imaging in the proximity of organs with high unspecific SPIO uptake such as liver or spleen.

References

[1] J. Franke, U. Heinen, H. Lehr, A. Weber, F. Jaspard, W. Ruhm, M. Heidenreich, and V. Schulz. System Characterization of a Highly Integrated Preclinical Hybrid MPI-MRI Scanner. *IEEE Trans. Med. Imag.*, 35(9):1993–2004, 2016. doi:10.1109/TMI.2016.2542041.

[2] N. Gdaniec, M. Hofmann, and T. Knopp. Limitations of Magnetic Particle Imaging Resolving Large Contrasts. In *International Workshop of Magnetic Particle Imaging*, page 81, 2016.

[3] M. Graeser, T. Knopp, M. Grüttner, T. F. Sattel, and T. M. Buzug. Analog receive signal processing for magnetic particle imaging. *Med. Phys.*, 40(4):042303, 2013. doi:10.1118/1.4794482.

[4] N. Panagiotopoulos, R. L. Duschka, M. Ahlborg, G. Bringout, C. Debbeler, M. Graeser, C. Kaethner, K. Lüdtke-Buzug, H. Medimagh, J. Stelzner, T. M. Buzug, J. Barkhausen, F. M. Vogt, and J. Haegele. Magnetic particle imaging: current developments and future directions. *Int. Journ. Nanomed.*, 10:3097, 2015. doi:10.2147/IJN.S70488.

[5] B. Gleich, J. Weizenecker, H. Timminger, C. Bontus, I. Schmale, J. Rahmer, J. Schmidt, J. Kanzenbach, and J. Borgert. Fast MPI Demonstrator with Enlarged Field of View. In *Proc. ISMRM*, volume 18, page 218, 2010.

[6] P. W. Goodwill, J. J. Konkle, B. Zheng, E. U. Saritas, and S. M. Conolly. Projection X-Space Magnetic Particle Imaging. *IEEE Trans. Med. Imag.*, 31(5):1076–1085, 2012. doi:10.1109/TMI.2012.2185247.

[7] P. Vogel, M. A. Rückert, P. Klauer, W. H. Kullmann, P. M. Jakob, and V. C. Behr. Traveling Wave Magnetic Particle Imaging. *IEEE Trans. Med. Imag.*, 33(2):400–407, 2014. doi:10.1109/TMI.2013.2285472.

[8] P. Vogel, S. Lother, M.A. Ruckert, W.H. Kullmann, P.M. Jakob, F. Fidler, and V.C. Behr. MRI Meets MPI: A Bimodal MPI-MRI Tomograph. *IEEE Trans. Med. Imag.*, 33(10):1954–1959, 2014. doi:10.1109/TMI.2014.2327515.

[9] P. Vogel, M. A. Rückert, P. Klauer, W. H. Kullmann, P. M. Jakob, and V. C. Behr. First in vivo traveling wave magnetic particle imaging of a beating mouse heart. *Phys. Med. Biol.*, 61(18):6620–6634, 2016. doi:10.1088/0031-9155/61/18/6620.

[10] P. Vogel, M. A. Rückert, and V. C. Behr. 3D-GUI Simulation Environment for MPI. In *International Workshop on Magnetic Particle Imaging*, 2016.

[11] P. Vogel, T. Kampf, M. A. Rückert, and V. C. Behr. Flexible and Dynamic Patch Reconstruction for Traveling Wave Magnetic Particle Imaging. *Intern. J. Magnetic Particle Imaging*, 2(2):1611001, 2016. doi:10.18416/ijmpi.2016.1611001.

[12] P. W. Goodwill and S. M. Conolly. The x-Space Formulation of the Magnetic Particle Imaging process: One-Dimensional Signal, Resolution, Bandwidth, SNR, SAR, and Magnetostimulation. *IEEE Trans. Med. Imag.*, 29(11):1851–1859, 2010. doi:10.1109/TMI.2010.2052284.

[13] V. R. Cross, R. K. Hester, and J. S. Waugh. Single coil probe with transmission-line tuning for nuclear magnetic double resonance. *Rev. Sci. Instrum.*, 47(12):1486–1488, 1976. doi:10.1063/1.1134560.